Acta Crystallographica Section D
Biological Crystallography
ISSN 0907-4449

Stabilization of active-site loops in NH_3-dependent NAD^+ synthetase from *Bacillus subtilis*

Yancho Devedjiev,[a]† Jindrich Symersky,[a] Raj Singh,[a] Marek Jedrzejas,[b] Christie Brouillette,[a,c] Wayne Brouillette,[a,d] Donald Muccio,[d] Debasish Chattopadhyay[a,e] and Larry DeLucas[a]*

[a]Center for Biophysical Sciences and Engineering, University of Alabama at Birmingham, Birmingham, AL 35294, USA, [b]Department of Microbiology, University of Alabama at Birmingham, Birmingham, AL 35294, USA, [c]Department of Biochemistry, University of Alabama at Birmingham, Birmingham, AL 35294, USA, [d]Department of Chemistry, University of Alabama at Birmingham, Birmingham, AL 35294, USA, and [e]Division of Geographic Medicine, School of Medicine, University of Alabama at Birmingham, Birmingham, AL 35294, USA

† Present address: Department of Molecular Physiology and Molecular Biophysics, University of Virginia, Charlottesville, VA 22906, USA.

Correspondence e-mail: delucas@cmc.uab.edu

Received 6 October 2000
Accepted 20 February 2001

PDB References: complex I, 1ifx; complex II, 1fyd; complex III, 1ee1; complex IV, 1ihb.

The NH_3-dependent NAD^+ synthetase (NADS) participates in the biosynthesis of nicotinamide adenine dinucleotide (NAD^+) by transforming nicotinic acid adenine dinucleotide (NaAD) to NAD^+. The structural behavior of the active site, including stabilization of flexible loops 82–87 and 204–225, has been studied by determination of the crystal structures of complexes of NADS with natural substrates and a substrate analog. Both loops are stabilized independently of NaAD and solely from the ATP-binding site. Analysis of the binding contacts suggests that the minor loop 82–87 is stabilized primarily by a hydrogen bond with the adenine base of ATP. Formation of a coordination complex with Mg^{2+} in the ATP-binding site may contribute to the stabilization of the major loop 204–225. The major loop has a role in substrate recognition and stabilization, in addition to the protection of the reaction intermediate described previously. A second and novel Mg^{2+} position has been observed closer to the NaAD-binding site in the structure crystallized at pH 7.5, where the enzyme is active. This could therefore be the catalytically active Mg^{2+}.

1. Introduction

The biosynthesis of NAD^+ is vitally important for both prokaryotic and eukaryotic organisms. The final step of the biosynthesis is the conversion of nicotinic acid adenine dinucleotide to NAD^+ catalyzed by NAD^+ synthetase. The conversion proceeds through an NAD–adenylate intermediate, which is formed in the presence of ATP and Mg^{2+}; subsequently, the intermediate is cleaved by ammonia to yield NAD^+ and AMP (Foster & Moat, 1980; Fig. 1). Functionally, NADS belongs to the family of amidotransferases and has been suggested to be a member of the newly recognized ATP pyrophosphatase family (Tesmer *et al.*, 1996). The enzyme is also required in bacterial spore germination and outgrowth (Albertini *et al.*, 1987). As the prokaryotic and eukaryotic forms of NADS differ in size, enzymatic activity and substrate requirements, NADS may be considered a potential target for development of a new class of antibiotics. Recently, it was found that NADS is also a general stress factor and its gene *NadE* is strongly induced in response to heat, salt, ethanol and deficiency of glucose (Antelmann *et al.*, 1997).

NADS consists of a tight homodimer with an α/β-subunit topology (Rizzi *et al.*, 1996). In the strictly NH_3-dependent NADS from *Bacillus subtilis*, the ATP-binding site is located at the classical α/β topological switch point, whereas a novel NaAD-binding site was found at the subunit interface in an adjacent cleft defined by the quaternary structure of NADS (Rizzi *et al.*, 1998). Stoichiometrically, there is one NaAD-

binding site and one ATP-binding site per subunit. Two active-site loops including residues 82–87 and 204–225 could not be localized in the apoenzyme structure, but become ordered upon binding of the substrates (Fig. 2). Presumably, the ordered loops prevent the NAD–adenylate intermediate from premature breakdown until the ammonia molecule carries out the final step of the reaction. Previously, it was suggested that PP_i, a leaving group in the first reaction step, participates in fixing the conformation of the loops and, in addition, that product release could take place only after all the substrates were bound, after which product release would be ultimately controlled by the conformation adopted by the two loops (Rizzi *et al.*, 1998). Similar conformational changes of active-site loops have been observed in other protein structures and studied extensively, for instance in HIV protease (Wagner, 1995). The mechanisms of substrate recognition, access control to the active site and release of reaction components have obvious importance for effective structure-based drug design. We have studied in more detail the structural changes of the NADS active site induced by natural substrates or substrate analogs. We found that both loops are stabilized independently of NaAD and we analyzed essential binding contacts of the stabilized loops. We show further implications for substrate recognition and stabilization, effect of a higher crystallization pH and discuss general outcomes for inhibitor design.

2. Experimental

2.1. Cloning, expression and purification of NADS

The 1 kbp *OutB* gene encoding *Bacillus subtilis* NADS (Nessi *et al.*, 1995) was cloned into a prokaryotic expression vector pET-21 (Novagen). After transformation in *E. coli* cells BL21(DH3) plysS, single colonies were propagated overnight at 310 K in Luria–Bertani (LB) medium containing 50 µg ml^{-1} ampicillin and 34 µg ml^{-1} chloramphenicol. Large-scale cultures (4–6 l) were grown at 310 K in LB media to OD = 0.8 at 600 nm and induced with 1 m*M* isopropylthio-D-galactoside (IPTG). The culture was then grown for another 4 h with constant shaking. Cells were harvested by centrifugation at 4500 rev min^{-1} for 15 min and stored at 193 K. The frozen cells were thawed and resuspended in buffer *A* (50 m*M* Tris, 1 m*M* EDTA, 0.1 m*M* PMSF, 1 m*M* DTT pH 7.5). The suspension was treated with DNase (1 mg ml^{-1}) for 30 min or sonicated to open the cells. After centrifugation at 30 000 rev min^{-1} for 30 min, a clear supernatant was loaded on a preparative Superdex-75 column (2.6 × 60 cm, Pharmacia) supported by an FPLC system using buffer *A* with 1% glycerol. NADS peak fractions were combined and further purified by ion-exchange chromatography on a Bio-Q column (BioRad) using a linear gradient of 0–0.5 *M* NaCl. Pooled NADS fractions were concentrated using a 10K ultrafiltration membrane (Amicon) and applied onto a Superdex-75 column as above. Approximately 25–30 mg of NADS was obtained from 1 l of the bacterial culture. The protein was better than 95% pure as judged by electrophoretic analysis. Purified NADS samples (5–6 mg ml^{-1}) were stored in 30% glycerol at 193 K for further use.

2.2. Crystallization of NADS complexes

Purified NADS was diluted 1:1 with 20 m*M* sodium acetate, 50 m*M* $MgCl_2$, 2.5 m*M* β-mercaptoethanol pH 6 and dialyzed against the same solution with the pH adjusted to 5.2. The dialyzed protein was concentrated to 15 mg ml^{-1}. Crystals were grown by the hanging-drop vapor-diffusion method at room temperature. The drops were prepared by mixing equal

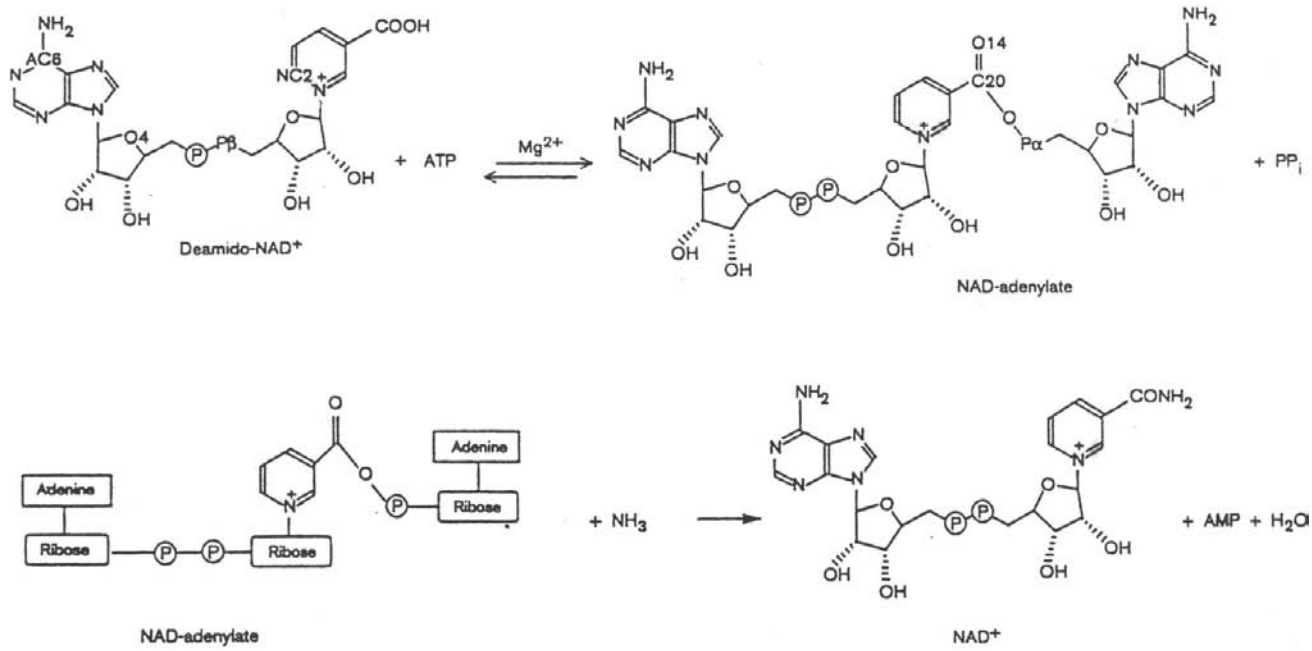

Figure 1
A scheme of the reaction catalyzed by NAD^+ synthetase.

volumes of the concentrated protein with a well solution consisting of 21–23%(*v*/*v*) PEG 400, 0.1 *M* sodium acetate pH 5.2, 50 m*M* $MgCl_2$ and the substrates as follows: complex I with 5 m*M* NaAD, complex II with 1 m*M* ATP, complex III with 5 m*M* NaAD and 0.5 m*M* ATP. All substrates were purchased from Sigma.

Complex IV with AMP-CPP (α,β-methylene-adenosine triphosphate) was prepared at a different pH. Purified NADS was dialyzed against 10 m*M* HEPES sodium salt pH 7.5 and concentrated to 20 mg ml^{-1}. Crystals were grown by micro-seeding (Hampton Research) using the same hanging-drop vapor-diffusion method. The well solution consisted of 20–26%(*v*/*v*) PEG 400, 50 m*M* HEPES sodium salt pH 7.5, 0.1 *M* $MgCl_2$ and 2 m*M* AMP-CPP. The seed-storage solution consisted of 25%(*v*/*v*) PEG 400, 0.1 *M* $MgCl_2$ and 50 m*M* HEPES sodium salt pH 7.5. Drops were made up of 3 µl of the concentrated protein, 3 µl of the well solution and 3 µl of the solution with microseeds at various dilutions.

Long prismatic crystals of approximate dimensions 0.1 × 0.2 × 0.5 mm can be grown in a few days using the methods described. The symmetry of the diffraction data and systematic absences showed unambiguously that crystals of the four complexes belong to the space group $P2_1$, with average unit-cell parameters a = 53.0, b = 86.4, c = 60.7 Å, β = 111.1°.

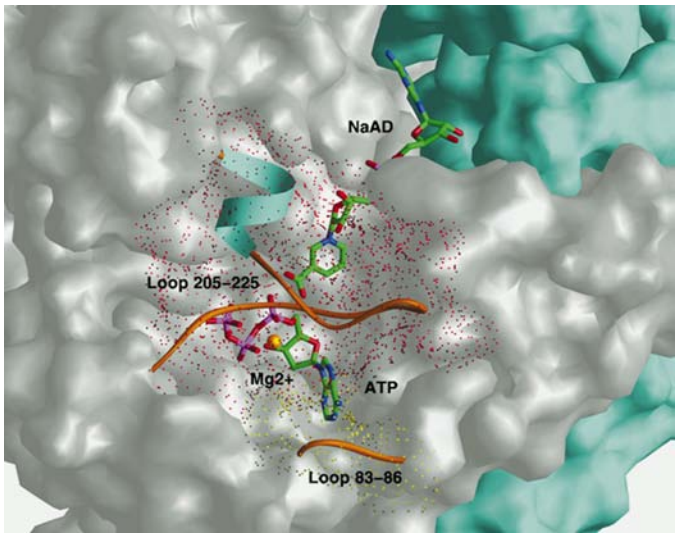

Figure 2
Molecular-surface representation of the active site of NAD^+ synthetase. Subunit *A* is in silver and subunit *B* in cyan. The flexible loops are shown as ribbon drawings and the substrates as stick models; the Mg^{2+} ion in position Mg(II) is shown as a golden sphere. The surface area of the minor loop is indicated by yellow dots, the surface of the major loop by red dots. This figure was prepared with *RIBBONS* (Carson, 1997).

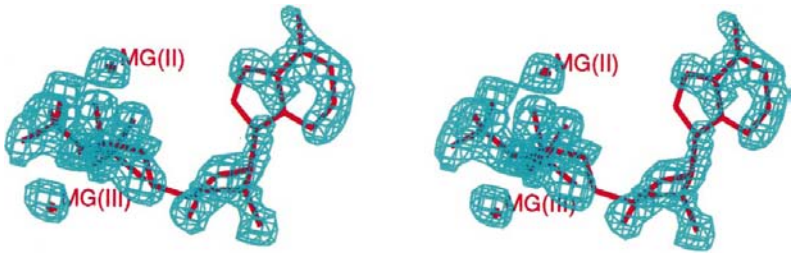

Figure 3
The initial $F_o - F_c$ map of complex IV contured at 3σ. Only the substrate electron density is shown, with two peaks interpreted as Mg^{2+} ions.

2.3. Data collection and processing

The diffraction data were collected on R-AXIS II, R-AXIS IV and MacScience image-plate area detectors powered by the Rigaku high-voltage generators RU-200 and HU-3R with a copper rotating anode and double-focusing mirrors. Data from complexes I and IV were collected at 120 K in a cryo-protectant consisting of the well solution with 35%(*v*/*v*) PEG 400 and the corresponding substrate. Crystals of the complexes II and III were mounted in glass capillaries and the data were collected at room temperature. Diffraction images were processed using the *HKL* package (Otwinowski & Minor, 1997) and the *CCP*4 program suite (Collaborative Computational Project, Number 4, 1994). An isomorphous NADS structure without the loops 82–87 and 204–225 and without ligands was used as an initial model (PDB code 1nsy; Rizzi *et al.*, 1996). Electron-density maps of the type $F_o - F_c$ and $2F_o - F_c$ were calculated with *X-PLOR* (Brünger, 1996) and *CNS* (Brunger *et al.*, 1998) and were displayed using *O* (Jones *et al.*, 1993). The simulated annealing and positional refinement were performed in *X-PLOR* or in *CNS*, the model building in *O* and the modeling in *CHAIN* (Sack, 1988). Generally, the refinement procedure included a simulated-annealing cycle and a positional refinement of the protein model. The substrates and ordered loops were then manually built to the $F_o - F_c$ and $2F_o - F_c$ maps (Fig. 3) and the positional refinement continued. A bulk-solvent correction was applied and water molecules added to the positions with a defined electron density and an acceptable geometry. Alternate cycles of the positional refinement and manual model building were continued until the *R* factors converged and no significant peaks were found in $F_o - F_c$ maps. The final models were analyzed with *PROCHECK* (Laskowski *et al.*, 1993).

3. Results and discussion

3.1. Binding of substrates

The diffraction data from four different substrate/analog complexes crystallized with NADS have been analyzed. The data collection and refinement statistics are summarized in Table 1. Complexes I–IV include the NADS homodimer with adducts as shown in Fig. 4. Crystals of the complexes I, II and III with natural substrates were prepared under similar conditions (see §2.2) at pH 5.2. The enzyme is not active at this pH. Complex IV with AMP-CPP, a pyrophosphatase-resistant (non-hydrolyzable) analog of ATP, was crystallized at the enzyme's active pH 7.5. The compound was chosen as a pseudosubstrate owing to its similarity to ATP and because it was known that it inhibits binding of

Table 1
Data-collection and refinement statistics.

Values in parentheses refer to the highest resolution shell.

NADS complex	I	II	III	IV
Data collection				
Unit-cell parameters				
a (Å)	53.1	53.4	53.0	52.6
b (Å)	86.1	87.2	86.7	85.4
c (Å)	61.1	61.2	60.5	60.2
β (°)	111.2	111.1	111.2	110.9
Resolution (Å)	20.0–2.3	20.0–2.25	20.0–2.0	30.0–1.9
Total No. of reflections	162585	84039	136657	112884
No. of unique reflections	24270	24198	30068	38796
R_{sym}† (%)	7.7 (27.8)	14.7 (38.9)	5.0 (15.6)	4.8 (15.4)
Completeness (%)	99.5 (79.2)	91.1 (72.6)	95.4 (83.0)	98.4 (98.8)
$I/\sigma(I)$	16.2 (3.5)	6.1 (2.1)	23.8 (7.8)	20.4 (7.6)
Temperature (K)	120	293	293	120
Refinement				
Resolution (Å)	6.0–2.3	6.0–2.25	6.0–2.0	30.0–1.9‡
No. of reflections used	23802	23738	29684	37902
R factor§ (%)	21.6	19.3	15.8	19.7
R_{free} (%)	27.2	27.6	21.9	24.7
R.m.s. bonds (Å)	0.012	0.012	0.013	0.005
R.m.s. angles (°)	2.1	1.8	2.2	1.09
Luzzati error (Å)	0.34	0.32	0.26	0.23
$\langle B \rangle$¶, subunit *A* (Å^2)	20.3	15.8	21.6	13.3
$\langle B \rangle$, subunit *B* (Å^2)	23.0	16.6	21.7	16.7

† $R_{sym} = \sum |I_i - \langle I_i \rangle| / \sum I_i$, where $\langle I_i \rangle$ is the average of the *i*th intensity measurement. ‡ Bulk-solvent correction applied before refinement in *CNS* (Brunger *et al.*, 1998). § $R = ||F_o| - |F_c|| / \sum |F_o|$, where $|F_o|$ and $|F_c|$ are the observed and calculated structure amplitudes, respectively. ¶ $\langle B \rangle$ is an overall temperature factor.

ATP to NADS. The structures are isomorphous, with order/disorder variations in active-site loops depending on the substrate. Although there are two equivalent active sites in the functional homodimer, three complexes were found, with uneven occupancies of their respective binding sites (Fig. 4). The only symmetrical complex crystallized is I, with one NaAD molecule bound in the proper site of each subunit, as expected. In complex II, only one AMP and one PP_i ion are found in the ATP-binding site of subunit *A*. Another asymmetric complex is III, in which subunit *A* is fully occupied by ATP and NaAD, while subunit *B* has only NaAD bound. Finally, complex IV has an AMP-CPP molecule bound in the ATP-binding site of the subunit *A* and subunit *B* is unoccupied. Rizzi *et al.* (1996) presented the complex AMP–PP_i–Mg^{2+} which was crystallized under similar conditions to our complex II. However, it has both ATP sites occupied with AMP and PP_i and in addition intact ATP molecules are bound to NaAD-binding sites of both subunits. Rizzi *et al.* (1998) have also shown an NAD–adenylate complex where both subunits are occupied by the reaction intermediate (Fig. 1). Both of these isomorphous complexes were crystallized at pH 5.2 and, importantly, considerably higher concentrations of ATP and NAD^+ were used in the crystallization, which yielded a full occupation of both subunits. We were using lower ATP and AMP-CPP concentrations to avoid binding of these substrates in NaAD sites and apparently this caused formation of asymmetric complexes. Remarkably, the crystal packing does not seem to block any of the unoccupied binding sites of subunit *B*. The overall temperature factors tend to be higher for the unoccupied *B* subunits (Table 1); however, the same trend is observed in Rizzi's complexes where both subunits are occupied evenly. It is also noteworthy that Rizzi *et al.* (1998) formed the NAD–adenylate complex by running the reaction backwards. The AMP from hydrolyzed ATP reacted with NAD^+ and the released ammonia was neutralized at the acidic pH 5.2.

Superpositions with Rizzi's complexes show the same mode of substrate binding in the present structures I–IV. The substrates (NaAD, ATP, AMP and AMP-CPP) bind as extended molecules to their proper sites, with only minor variations in local conformations and binding contacts. The terminal phosphates of ATP and AMP-CPP are folded into a complex with Mg^{2+}. Although complex IV was crystallized at pH 7.5, there is no apparent difference in binding of AMP-CPP to the ATP-binding site compared with the structures at pH 5.2. The data also show that in complex II the ATP molecule has been hydrolyzed to AMP and PP_i, while in complex III there is an intact ATP molecule in subunit *A*, with no covalent connection to NaAD. This is somewhat surprising, as Rizzi *et al.* (1996) have also shown that the ATP-binding site was occupied by AMP and PP_i. In complex III, however, the

NADS complex	pH	Subunit *A*							Subunit *B*						
		NaAD site	ATP site	Mg(I)	Mg(II)	Mg(III)	Loop 82-87	Loop 204-225	NaAD site	ATP site	Mg(I)	Mg(II)	Mg(III)	Loop 82-87	Loop 204-225
Rizzi *et al.* (1996)	5.2	**ATP**	**AMP PPi**	**Mg^{2+}**	Mg^{2+}		Order.	Order.	**ATP**	**AMP PPi**	**Mg^{2+}**	Mg^{2+}		Order.	Order.
Rizzi *et al.* (1998)	5.2	**NAD-adenylate**		**Mg^{2+}**	**Mg^{2+}**		Order.	Order.	**NAD-adenylate**		**Mg^{2+}**	**Mg^{2+}**		Order.	Order.
I	5.2	**NaAD**					Disord.	Disord.	**NaAD**					Disord.	Disord.
II	5.2		**AMP PPi**	Mg^{2+}	**Mg^{2+}**		Order.	Order.		AMP PPi	Mg^{2+}	Mg^{2+}		Disord.	Disord.
III	5.2	**NaAD**	**ATP**	Mg^{2+}	**Mg^{2+}**		Order.	Order.	**NaAD**	ATP	Mg^{2+}	Mg^{2+}		Disord.	Disord.
IV	7.5		**AMP-CPP**	Mg^{2+}	**Mg^{2+}**	**Mg^{2+}**	Order.	Order.		AMP-CPP	Mg^{2+}	Mg^{2+}	Mg^{2+}	Disord.	Disord.

Figure 4
Occupation of binding sites in the crystal structures of NAD^+ synthetase and order/disorder status of the active-site loops. The ligands found are in shaded boxes in bold. Expected and/or missing ligands are indicated in normal type. NaAD, nicotinic acid adenine dinucleotide; AMP, adenosine monophosphate; PP_i, pyrophosphate ion; ATP, adenosine triphosphate; AMP-CPP, α,β-methylene-adenosine triphosphate.

ATP-binding site of subunit *A* is completely closed by the bound NaAD, whose carboxyl group is in a hydrogen-bonding contact with the α-phosphate. This may block the enzymatic hydrolysis of ATP, the mechanism of which is unknown. At the same time, the adenylation step is blocked because of the low pH.

An important difference from the NAD–adenylate complex is observed for NaAD molecules in complexes I (both subunits) and III (subunit *B*), where the nicotinosyl moiety is clearly disordered (Figs. 4 and 5). While the ADP part has a normal electron density and temperature factors of 20–40 Å^2, the nicotinosyl moiety has a broken or a missing electron density and temperature factors of 60–80 Å^2. Apparently, the contacts with proximal residues Phe167 and Asp173 are not sufficient to stabilize it. As can be seen in subunit *A* of III, the nicotinosyl is stabilized by contacts with loop 204–225, which becomes ordered upon binding ATP, not NaAD. The N-ribose diol O atoms of NaAD are hydrogen bonded to the carboxylate O atoms of Glu223 and additional contacts are formed with Ala209 and Leu211. A similar conformation and contacts are observed for the nicotinosyl moiety in the NAD–adenylate complex. It shows that the loop 204–225 not only shields the substrates from solvent but also stabilizes NaAD for the adenylation step.

The NADS natural substrates, NaAD and ATP, are identical in their ADP parts. Consequently, both ATP- and NaAD-binding sites have to recognize ADP. In fact, Rizzi *et al.* (1996) have shown that ATP can also occupy the NaAD-binding site. On the other hand, because we did not observe NaAD in the ATP-binding site, it appears that the enzyme can efficiently distinguish between NaAD and ATP. Modeling shows that the larger NaAD molecule does not fit easily into the ATP-binding site unless the loop 204–225 is completely removed. Thus, NADS may distinguish NaAD from ATP based on the difference in their size. This is apparently facilitated by the loop 204–225, which interferes with binding of the larger NaAD molecule in the ATP-binding site.

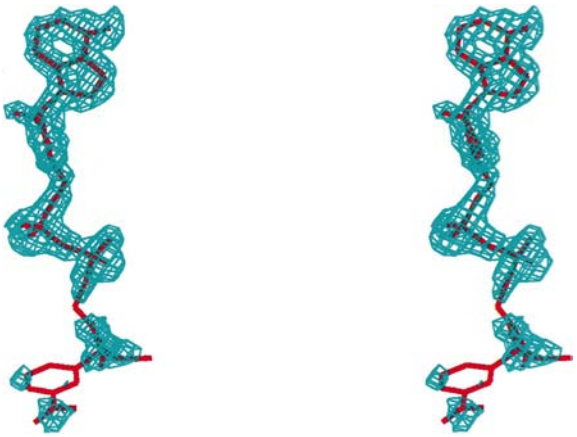

Figure 5
The final 2 $F_o - F_c$ map of complex I contoured at 1σ. Only the electron density of NaAD in subunit *A* is shown, with apparent disorder in the nicotinosyl part of the molecule.

3.2. Binding of Mg^{2+}

Because of their essential role in catalysis, positions of two magnesium sites Mg(I)[1] and Mg(II) have been well established in the NAD–adenylate complex at pH 5.2 (Rizzi *et al.*, 1998). Typically, atoms involved in the coordination of Mg^{2+} are arranged in a regular octahedron. However, an ideal octahedral coordination is only seen in well refined structures at high resolution. In structure I, with only NaAD bound, we did not find any stronger peaks of electron density that could be interpreted as Mg^{2+}. Also, in subunit *B* of III, occupied by NaAD, no magnesium was found. An apparently strong electron-density peak in the ATP-binding site with bound AMP and PP_i was found in complex II (Fig. 4). It coincides with position Mg(II) in the NAD–adenylate complex and is coordinated with one O atom of the α-phosphate, the carbonyl O atom of Thr208, two O atoms of the pyrophosphate (PP_i) and two water molecules (Fig. 6). No electron density was found in the position Mg(I) in contrast to Rizzi *et al.* (1996). Structure III has also been found with one Mg atom in position Mg(II) of subunit *A*. This site is octahedrally coordinated with three O atoms of the α-, β- and γ-phosphate of ATP, two O atoms from neighboring water molecules and a carbonyl O atom of Thr208 from the ordered loop 204–225 (Fig. 6). Finally, complex IV was found to have two Mg^{2+} ions in the ATP-binding site (Fig. 3). The first coincides with Mg(II) in the NAD–adenylate complex and the coordination sphere includes the same atoms described above, *i.e.* most importantly the carbonyl O atom of Thr208. The second magnesium, however, is shifted 2.6 Å from Mg(I) towards the NaAD-binding site and has an octahedral coordination with the α-phosphate O atom, the carboxylate O atom of Glu162 and four water molecules (Fig. 6). This is a novel magnesium site that has not been observed before in the structures crystallized at pH 5.2. We denote this site Mg(III). Remarkably, binding of Mg^{2+} is always associated with phosphate O atoms in the ATP-binding site and, more importantly, position Mg(II) in structures II, III, IV and in the NAD–adenylate complex is correlated with ordered loop 204–225, which is linked to the magnesium through the carbonyl O atom of Thr208.

Conformations of amino-acid residues forming the ATP-binding site are almost identical in the complexes studied, except for the side chain of Glu162, which shows significant variations. The high-resolution NAD–adenylate complex has the Glu162 side chain engaged in coordination with Mg(I). In structures I, II and III, the side chain of Glu162 is flipped approximately 180° around the bond between α and β C atoms and there is no magnesium found in the position Mg(I). In complex IV, the Glu162 assumes a new conformation coordinated to Mg(III) (Fig. 6). The diversity of these conformations may reflect different ionization states of Glu162 and of the phosphates which depend on pH and solvent accessibility. The most significant for the catalysis may be the finding that complex IV crystallized at pH 7.5 has a new magnesium

[1] Magnesium sites are denoted Mg(I), Mg(II) and Mg(III) following Rizzi *et al.* (1998) and should not be confused with oxidation states.

site that is within 3.6 Å of the position where NaAD binds. The optimal pH for the enzymatic reaction is 8.5 and it was proposed that the adenylation step of the reaction is carried out through an electron-withdrawing effect of Mg^{2+} ions present in the active site (Rizzi *et al.*, 1998). Thus, as the nearest magnesium ion, Mg(III) may well assist in charge compensation and/or electron withdrawing from the carboxyl group of NaAD. However, in the absence of bound NaAD, it is not clear if Mg(III) is the catalytic site or just an intermediate site.

3.3. Active-site loops

The order/disorder changes of active-site loops 82–87 and 204–225 depend on substrates. In structure I, the loops are disordered, as was observed in the apoenzyme structure. Disordered active-site loops are also observed in subunit *B* of all complexes with an unoccupied ATP-binding site (Fig. 4). Apparently, binding of NaAD has no ordering effect on the loops and, conversely, the disordered loop 204–225 cannot stabilize the conformation of the nicotinosyl moiety. In contrast, in subunit *A* of complexes II, III and IV, both loops can be unambiguously identified and refined. Ordering of the loops is triggered solely from the ATP-binding site and there are no allosteric effects between the subunits. This was not clear from Rizzi's structures with all binding sites occupied (Fig. 4). Conformations of the ordered loops are essentially the same in all studied complexes. Also, there is a common pattern in binding contacts between the loops and substrates, and between the loops and other protein residues. Only one significant contact is found between the adenine base and the ordered loop 82–87. It is a hydrogen bond that connects the adenine amino group with the carbonyl O atom of the side chain of Gln84. The distance N···O varies between 2.6 and 2.9 Å. Other significant hydrogen bonds are between the side chains of Gln84 and Arg78, Glu87 and Arg78. The second loop 204–225 is linked through the carbonyl O atom of Thr208 to the coordination site Mg(II) described in §3.2 and shown in Fig. 6. In addition, there is also one direct hydrogen bond between the peptide N atom of Thr208 and the O atom of the γ phosphate. However, the distance N···O is longer than 3 Å in all available structures. The loop 204–225 has only three hydrogen bonds to other protein residues. These connect side chains between Lys205 and Asp89, Asp213 and Lys135, and Gln217 and Asp86. Based on interatomic distances, none of these could be characterized as a 'strong' hydrogen bond or a salt bridge. Conformations of the residues Arg78, Asp89 and Lys135 are the same in the apoenzyme structure and do not seem to be induced by the bound ATP in the complex structures.

It appears that the minor loop 82–87 is stabilized by the adenine base of ATP through the only hydrogen-bonding contact between the amino group and the side chain of Gln84. We have shown several contacts that may contribute to stabilization of the major loop 204–225. However, in all studied structures they have relatively poor binding geometry. On the other hand, Mg(II) has a well formed octahedral coordination which is in keeping with the known coordination behavior of this cation in proteins as well as in coordination complexes (Carugo *et al.*, 1993). Therefore, the coordination with Mg^{2+} through the carbonyl O atom of Thr208 appears to be important in stabilization of the loop 204–225.

4. Conclusions and outlook

Although ordered active-site loops were observed in the complexes of NADS with ATP (Rizzi *et al.*, 1996) and with the NAD–adenylate intermediate (Rizzi *et al.*, 1998), little was suggested on the mechanism and the roles in substrate recognition and stabilization were not established. We found that NaAD does not stabilize the loops and showed which contacts in the ATP-binding site may be most important in stabilization of the loops. We have also shown how the loop 204–225 assists in distinguishing between NaAD and ATP and how the ordered loop 204–225 stabilizes the nicotinosyl moiety of NaAD. Finally, we found that higher pH does not affect substrate binding in the ATP-binding site or the stabilization of active-site loops, but it does affect the position of one magnesium ion and the conformation of Glu162. While the Mg(II) site is still involved in stabilization of the loop 204–225, the novel Mg(III) site may be responsible for an

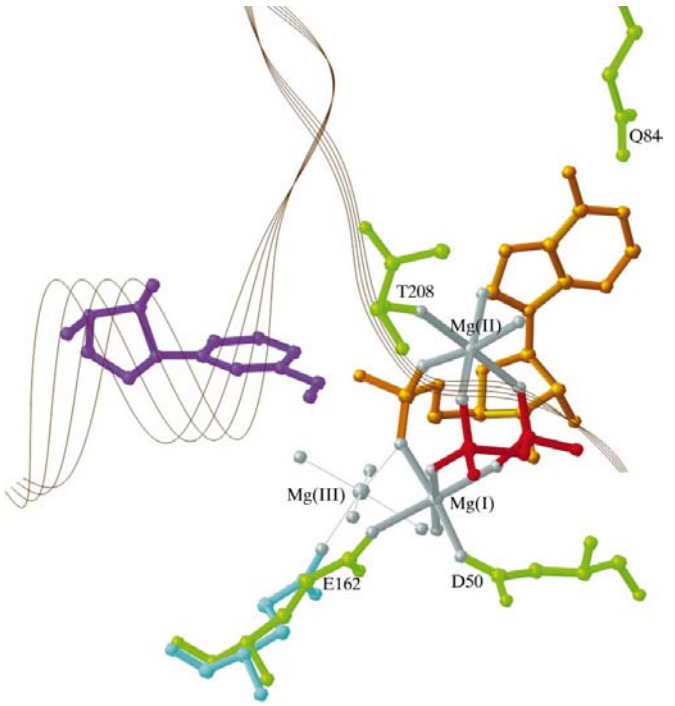

Figure 6
Coordination of Mg^{2+} in the ATP-binding site of NAD^+ synthetase. The nicotinosyl moiety of NaAD is shown in violet, AMP in gold and PP_i in red; Mg^{2+} with coordinated O atoms are shown in silver, relevant amino-acid residues are in green and the loop 204–225 is indicated by thin brown lines. Positions Mg(I), Mg(II) and Mg(III) are explained in the text. Coordination of the new Mg(III) position is indicated by thin silver lines. The new conformation of Glu162 at pH 7.5 is shown in cyan. ATP and AMP-CPP are not shown for clarity. Prepared with *RIBBONS* (Carson, 1997).

electron-withdrawing effect that facilitates the adenylation step.

The future design of NADS inhibitors should consider that both NaAD- and ATP-binding sites are designed to accommodate ADP. A classic approach may simply seek a compound which would eventually bind tighter than natural substrates to either the NaAD- or ATP-binding site regardless of the active-site loops. It seems unlikely that a single large molecule could occupy both NaAD- and ATP-binding sites because of steric interference with the active-site loops. Moreover, such a compound would probably not be useful as a drug. The most commonly used drugs have molecular weights less than 500, to provide reasonable opportunities for absorption and distribution throughout the body. A simple geometrical complementarity of an inhibitor molecule with the active site will probably not be sufficient for tight binding because ADP possesses diverse but distinct functions including charged phosphates, a relatively neutral ribose and a heteroaromatic adenine base with a strong potential for hydrogen bonds and stacking interactions. The synthesis of such compounds with multiple functions is, however, not straightforward. Binding to the ATP-binding site is apparently more specific compared with the NaAD-binding site. Considerably higher substrate concentrations are necessary for a full occupation of the NaAD-binding site in the crystal structures compared with the ATP-binding site. In addition, the nicotinosyl moiety of NaAD is not recognized until the loop 204–225 becomes ordered. It suggests that inhibitor binding to the NaAD-binding site may also be hampered. An efficient inhibitor design may attempt to develop compounds similar to AMP-CPP that can bind in the ATP-binding site, stabilize the loops and thereby prevent ATP binding. In this respect, magnesium coordination compounds with a flexible ligand-exchange potential may be worth exploring.

The authors thank Drs Galizzi and Rizzi for the *B. subtilis* NAD^+ synthetase cDNA and M. Rice for help in manuscript preparation. This work was supported in part by the Defense Advanced Research Proposal Agency.

References

Albertini, A., Caramori, T., Henner, D., Ferrari, E. & Galizzi, A. (1987). *J. Bacteriol.* **169**, 1480–1484.
Antelmann, H., Schmid, R. & Hecker, M. (1997). *FEMS Microbiol. Lett.* **153**, 405–409.
Brünger, A. T. (1996). *X-PLOR Version* 3.85. *A System for X-ray Crystallography and NMR.* New Haven, Connecticut: Yale University Press.
Brunger, A. T., Adams, P. D., Clore, G. M., DeLano, W. L., Gros, P., Grosse-Kunstleve, R. W., Jiang, J.-S., Kuszewski, J., Nilges, M., Pannu, N. S., Read, R. J., Rice, L. M., Simonson, T. & Warren, G. (1998). *Acta Cryst.* D**54**, 905–921.
Carson, M. (1997). *Methods Enzymol.* **277**, 493–505.
Carugo, O., Djinovic, K. & Rizzi, M. (1993). *J. Chem. Soc. Dalton Trans*, pp. 2127–2135.
Collaborative Computational Project, Number 4 (1994). *Acta Cryst.* D**50**, 760–763.
Foster, J. W. & Moat, A. G. (1980). *Microbiol. Rev.* **44**, 83–105.
Jones, T. A., Bergdoll, M. & Kjeldgaard, M. (1993). *Crystallographic Computing and Modeling Methods in Molecular Design.* New York: Springer.
Laskowski, R. A., MacArthur, M. W., Moss, D. S. & Thornton, J. M. (1993). *J. Appl. Cryst.* **26**, 283–291.
Nessi, C., Albertini, A. M., Speranza, M. L. & Galizzi, A. (1995). *J. Biol. Chem.* **270**, 6181–6185.
Otwinowski, Z. & Minor, W. (1997). *Methods Enzymol.* **276**, 307–326.
Rizzi, M., Bolognesi, M. & Coda, A. (1998). *Structure*, **6**, 1129–1140.
Rizzi, M., Nessi, C., Mattevi, A., Coda, A., Bolognesi, M. & Galizzi, A. (1996). *EMBO J.* **15**, 5125–5134.
Sack, J. S. (1988). *J. Mol. Graph.* **6**, 224–225.
Tesmer, J. J. G., Klem, T. J., Deras, M. L., Davisson, V. J. & Smith, J. L. (1996). *Nature Struct. Biol.* **3**, 74–86.
Wagner, G. (1995). *Nature Struct. Biol.* **2**, 255–257.